Incorporation of Transition Metal Ions into MeAPO/MeAPSO Molecular Sieves

A. M. Prakash, Martin Hartmann,† Zhidong Zhu, and Larry Kevan*

Department of Chemistry, University of Houston, Houston, Texas 77204

Received: October 27, 1999

The synthetic incorporation of transition metal ions into aluminophosphate and silicoaluminophosphate molecular sieve frameworks is studied by electron spin−echo modulation (ESEM) spectroscopy. Based mainly on bulk chemical composition of the product, it has been suggested that divalent and trivalent metal ions such as Mn(II), Co(II), Cr(III), and Fe(III) substitute for framework aluminum sites. On the basis of ^{31}P ESEM results, we originally suggested a framework phosphorus site for the incorporation of metal ions such as Ni(II) and Cr(III) in NiAPSO-5 and CrAPSO-5 molecular sieves. This site was later supported for other metal ions such as Ti(IV), V(IV), and Cu(II). In this work, we have extended such studies to Mn(II) and Fe(III) to better understand the metal substitution sites in $AlPO_4$ frameworks. Irrespective of the particular metal ion, the ^{31}P ESEM spectra of MeAPO/MeAPSO molecular sieves can be interpreted best on the basis of metal incorporation at a framework phosphorus site. Strong ^{27}Al modulations are also observed for these materials, which supports the ^{31}P ESEM result that incorporated metal ions are located nearer to aluminum than phosphorus.

Introduction

Synthesis of metal incorporated aluminophosphate and silicoaluminophosphate molecular sieves (MeAPO/MeAPSO) was first reported in 1986.[1,2] The metal ion, Me, can be either transition metal ions such as Ti, V, Cr, Mn, Co, or Ni or nontransition metal such as Mg. The MeAPO and MeAPSO molecular sieves constitute a new class of catalysts exhibiting both acid and metal sites in microporous environments. The incorporated metal ion often shows special catalytic activities different from those observed for metal ions residing in ion-exchanged sites inside the channels or cages of a molecular sieve or for a simple physical mixture of metal oxide and molecular sieve. This has been demonstrated for several catalytic reactions.[3−6] Because of their interesting catalytic properties, these materials have been studied by various physicochemical methods in order to understand the location and specific mechanism of incorporation of the metal ion.[7,8] Among the methods that have been used to characterize MeAPO/MeAPSO materials are IR and UV−vis spectroscopy, ^{27}Al, ^{29}Si, and ^{31}P MAS NMR, electron spin resonance (ESR), electron spin echo modulation (ESEM) spectroscopy, X-ray absorption (EXAFS and XANES) spectroscopy, Mössbauer spectroscopy, X-ray photoelectron spectroscopy, scanning electron microscopy, energy dispersive analysis of X-rays (EDAX), chemical analysis, measurement of acidity by temperature-programmed ammonia desorption, test of sorption and ion-exchange capacity, catalytic test reactions, and powder and single crystal diffraction methods. Except for a few techniques such as ESEM and X-ray absorption spectroscopy, the other methods do not directly probe the local environment of the metal ion but give global information regarding the material under consideration. The various data, however, support the idea that, under controlled synthesis procedures, molecular sieves with highly dispersed metal ions in their framework can be prepared. In an ideal $AlPO_4$ framework, metal ions can be incorporated at either framework aluminum or phosphorus sites. Based primarily on chemical analysis of the synthesized materials, it has been suggested that divalent metal ions such as Co(II), Mn(II), and Zn(II) are incorporated in a framework aluminum site.[9] However, recent ESR and ESEM studies on divalent nickel containing $AlPO_4$ materials suggest that Ni(II) substitutes for a framework phosphorus site.[10−12] The incorporation mechanism for higher valent metal ions such as Ti(IV), V(IV), and Cr(V) is also under debate. In their studies on the synthesis and characterization of VAPO-5 molecular sieve, Montes et al.[13] and Jhung et al.[14] suggested that vanadium substitutes for framework phosphorus sites, whereas Rigutto and Van Bekkum[15] suggested substitution into an aluminum site. Our earlier ESR and ESEM studies on VAPO-5, TAPO-5, and CrAPSO-5 molecular sieves suggest metal substitution for framework phosphorus sites.[16−18]

The local coordination of metal ions in MeAPO or MeAPSO molecular sieve frameworks is also another matter for discussion. X-ray absorption studies (EXAFS and XANES) have been used to obtain information about the oxygen coordination number and its distance from the metal ions in some MeAPO/MeAPSO molecular sieves.[19−23] From extended oscillations of the absorption coefficient in the high-energy part of the spectrum, it is possible to calculate the coordination number and interaction distance around the metal ion. In the case of NiAPO-5 and NiAPSO-34 molecular sieves, it has been suggested that nickel is incorporated into the framework in a distorted, tetrahedrally bonded state.[20] Also, EXAFS studies of zinc, manganese, and cobalt substituted aluminophosphate molecular sieves indicate four coordination for these cations.[21−23] Since EXAFS measurements provide only information about the oxygen coordination, it cannot distinguish metal substitution between phosphorus or aluminum sites. Most of these reports, however, *assume* metal substitution at framework aluminum sites based on bulk chemical analysis. The same is true for single-crystal X-ray diffraction studies on MeAPO materials.

† Present address: Department of Chemistry, Chemical Technology, University of Kaiserslautern, P. O. Box 3049, D- 67656 Kaiserslautern, Germany.

10.1021/jp993818j CCC: $19.00
Published on Web 01/29/2000

The crystal structure of a number of MeAPO molecular sieves has been determined by single-crystal X-ray diffraction studies.[24,25] Structure refinement has been done on the assumption that the metal substitutes for an aluminum site. The X-ray analysis has certain limitations too. The low metal content of MeAPO materials often renders the method incapable of locating the metal ion. Even in materials with higher metal concentration, the technique often fails to provide any direct information about the metal to oxygen coordination number and distance because of a random distribution of the metal at various crystallographic sites or due to the presence of extraframework metal species.

ESR and ESEM spectroscopies have been extensively used to probe the environment of various transition metal ions in MeAPO/MeAPSO molecular sieves.[8] While ESR can be used to deduce the local symmetry of the transition metal ion, analysis of the ESEM signal yields the number and distance of associated ligands.[8,26] In MeAPO/MeAPSO molecular sieves, analysis of the ^{27}Al and ^{31}P modulation often yields direct information about the metal ion location. The usefulness of these techniques has been demonstrated in a number of materials.[16−18,27] This report evaluates ESEM studies on metal ion incorporation into $AlPO_4$/SAPO materials and includes new data on Mn(II) and Fe(III) incorporation into these materials.

Experimental Section

First-row transition metal ions including Ti, V, Cr, Mn, Fe, Ni, and Cu are investigated for their specific incorporation mechanism into aluminophosphate/silicoaluminophosphate frameworks. The aluminophosphate structure type AFI is selected because the AFI structure type can be successfully synthesized in all compositional variants such as aluminophosphate ($AlPO_4$-5), silica (SSZ-24), silicoaluminophosphate (SAPO-5), metal aluminophosphate (MeAPO-5), and metal silicoaluminophosphate (MeAPSO-5). Moreover, the AFI structure can be prepared with varying metal concentrations in the framework.

All MeAPO-5 and MeAPSO-5 molecular sieves were synthesized by hydrothermal procedures using standard recipes. The metal ion concentration in various samples was kept very low so as to ensure high dispersion of the metal ion and avoid formation of any metal clusters. This is required to achieve electron spin relaxation times long enough so that electron spin echoes can be detected. Syntheses of TAPO-5, VAPO-5, CrAPSO-5, NiAPSO-5, and CuAPO-5 were reported earlier.[10,16−18,27] Samples of MnAPO-5 and FeAPO-5 were prepared by using triethylamine (TEA) as the organic structure directing molecule. On the basis of preliminary experiments, the following gel compositions were optimized. The metal sources used

$$\text{MnAPO-5: } 2.0\text{TEA}/0.005\text{MnO}/1\text{Al}_2\text{O}_3/1\text{P}_2\text{O}_5/50\text{H}_2\text{O}$$

$$\text{FeAPO-5: } 2.0\text{TEA}/0.005\text{Fe}_2\text{O}_3/1\text{Al}_2\text{O}_3/1\text{P}_2\text{O}_5/50\text{H}_2\text{O}$$

were manganese acetate tetrahydrate (Sigma) and ferrous sulfate heptahydrate (Fisher), respectively, for MnAPO-5 and FeAPO-5. In a typical synthesis, 4.85 g of pseudoboehmite (Catapal-B: Vista, 70 wt % Al_2O_3) was slurred in 12.5 g deionized water. The slurry was stirred for 2 h. A second solution was prepared by mixing 7.69 g of phosphoric acid (Aldrich, 85%) diluted in 5 g of water and the corresponding metal salts (0.04 g manganese acetate or 0.09 g ferrous sulfate) dissolved in 2 g of water. The second solution was added dropwise to the alumina slurry. Another 9 g of water was also added to this mixture. The mixture was then kept stirring for 3 h. To this mixture, 6.75 g of triethylamine (Aldrich, 99%) was then added slowly. The final mixture was stirred for another 2 h to make it highly homogeneous. The pH of the gel at this stage is about 6.5. About 10 mL each of the gel was then transferred to 20 mL Teflon-lined autoclaves and heated to 473 K for 24 h without agitation. After crystallization, the product was separated from the mother liquor, washed with water and dried at 340 K overnight. The as-synthesized samples were calcined by raising the temperature slowly to 823 K in flowing O_2 and keeping the sample at this temperature for 16 h for removal of the organic template.

Sample Treatment and Measurements. X-ray powder diffraction patterns were recorded on a Philips PW 1840 X-ray diffractometer using Cu Kα radiation. The spectra were collected stepwise in the $4° \leq 2\theta \leq 50°$ angular region. Chemical analysis of the samples was carried out by electron microprobe analysis on a JEOL JXA-8600 spectrometer. For each sample, the composition was analyzed on a number of crystals. In the particular cases of MnAPO-5 and VAPO-5, the concentration of these metal ions was below the detection limit for some measurements. For ESR and ESEM measurements, both as-synthesized and calcined samples were loaded into 3 mm o.d. $\times$ 2 mm i.d. Suprasil quartz tubes. As-synthesized samples were analyzed without any pretreatment. The calcined samples were first evacuated to a final pressure of 10^{-4} Torr at 295 K overnight. The samples were then gradually heated under vacuum from 295 to 673 K and kept at this temperature for 16 h for dehydration and sealed. Then ESR spectra were measured at 77 K to study the change in behavior by this thermal treatment. Characteristic ESR signals corresponding to V(IV), Cr(III) or Cr(V), Fe(III), Mn(II), and Cu(II) are observed in VAPO-5, CrAPSO-5, FeAPO-5, MnAPO-5, and CuAPO-5 molecular sieves in their as-synthesized, calcined, or dehydrated forms. No ESR signal was observed in the corresponding samples of NiAPSO-5 and TAPO-5 molecular sieves. Paramagnetic Ni(I) and Ti(III) species were generated in NiAPSO-5 and TAPO-5 samples by hydrogen treatment or γ-ray irradiation. Before exposure to reducing agents, dehydrated samples were first treated with O_2 at 773 K for 6−8 h followed by evacuation at this temperature. To study hydration−dehydration behavior of manganese and iron, the dehydrated MnAPO-5 and FeAPO-5 samples were exposed to the room-temperature vapor pressure of D_2O (Aldrich Chemical). These samples were then sealed and kept at room temperature for 24 h before ESR and ESEM measurements.

ESR spectra were recorded with a Bruker ESP-300 X-band spectrometer at 77 K. The magnetic field was calibrated with a Varian E-500 gaussmeter. The microwave frequency was measured by a Hewlett-Packard HP 5342A frequency counter. ^{31}P and ^{27}Al ESEM spectra were measured at temperatures between 4.5 and 10 K with a Bruker ESP 380 pulsed ESR spectrometer. Three pulse echoes were measured by using a $\pi/2-\tau-\pi/2-T-\pi/2$ pulse sequence as a function of time T to obtain the time domain spectrum. For measurement of a particular nucleus, modulations from other nuclei were minimized by choosing the τ value accordingly depending on the magnetic field position.[26] The ^{27}Al and ^{31}P ESEM spectra of various MeAPO-5/MeAPSO-5 materials were measured at a magnetic field showing the maximum absorption in the ESR spectra of the corresponding paramagnetic ions. The spectra were measured on dehydrated or reduced samples. Phosphorus modulations were analyzed by a spherical approximation for powder samples in terms of N nuclei at distance R with an isotopic hyperfine coupling A_{iso}.[26] The best-fit simulation of an ESEM signal is found by varying the parameters until the sum of the squared residuals between the simulated and experimental

TABLE 1: Elemental Framework Composition of Various MeAPO/MePSO-5 Molecular Sieves as Obtained by Electron Microprobe Analysis

sample type	$(Me_x\ Al_y\ P_z\ Si_w)O_2$[a]
TAPO-5	$(Ti_{0.020}Al_{0.500}\ P_{0.480})O_2$
VAPO-5	$(V_{0.001}Al_{0.506}P_{0.493})O_2$
CrAPSO-5	$(Cr_{0.004}Al_{0.496}P_{0.461}Si_{0.037})O_2$
MnAPO-5	$(Mn_{<0.001}Al_{0.505}P_{0.496})O_2$
FeAPO-5	$(Fe_{0.003}Al_{0.505}P_{0.495})O_2$
NiAPSO-5	$(Ni_{0.010}Al_{0.500}P_{0.470}Si_{0.020})O_2$
CuAPO-5	$(Cu_{0.030}Al_{0.510}P_{0.460})O_2$

[a] In MeAPO-5 samples $x + y + z = 1$ and in MeAPSO-5 samples $x + y + z + w = 1$.

spectra is minimized. Typical accuracies are N to the nearest integer, ±0.1 Å for R and ±10% for A_{iso}.

Results and Discussion

The crystallinity and phase purity of the samples was confirmed by powder X-ray diffraction. The chemical analysis of calcined samples is given in Table 1. Since the metal concentration is generally low, sometimes even below the instrumental detection limit, it is difficult to draw any conclusions from these results about the specific site of metal ion incorporation. This is particularly true for MnAPO-5 and VAPO-5 samples where the ratio Me/(Me + Al + P) is 0.001 or less.

As-synthesized and calcined, hydrated samples of VAPO-5, MnAPO-5, FeAPO-5, and CuAPO-5 show characteristic ESR signals due to the corresponding paramagnetic ions V(IV), Mn(II), Fe(III), and Cu(II) having coordination with one or more water molecules. CrAPSO-5 shows a characteristic ESR signal due to Cr(III) in its as-synthesized form and due to Cr(V) in its calcined, dehydrated form. Detailed ESR studies on the location and adsorbate interactions of Ti(III), V(IV), Cr(V), Ni(II), and Cu(II) in TAPO-5, VAPO-5, CrAPSO-5, NiAPSO-5, and CuAPO-5 have been reported.[10,16−18,27] Figures 1 and 2 show ESR spectra of MnAPO-5 and FeAPO-5 observed after various treatments. As-synthesized MnAPO-5 shows an ESR signal with resolved hyperfine lines. The ESR parameters of $g_{av} = 2.006$ and $A_{av} = 0.0084\ cm^{-1}$ are consistent with that obtained from axially symmetric divalent manganese species in molecular sieves and other solids.[28] The signal is more resolved in a calcined, hydrated sample and shows additional lines between the six main hyperfine lines. These additional lines are assigned to $\Delta m_I = \pm 1$ forbidden transitions according to previous Mn(II) ESR studies.[29] A slight increase in the hyperfine splitting is observed in calcined, hydrated MnAPO-5 ($g_{av} = 2.007$ and $A_{av} = 0.0089\ cm^{-1}$). It should be noted that as-synthesized MnAPO-5 contains the organic template in addition to water molecules. Thus, the observed differences in ESR spectra between as-synthesized and calcined, hydrated MnAPO-5 probably arise from the presence of the organic species. Upon dehydration of a calcined, hydrated sample, the ESR signal intensity decreases significantly due to loss of water ligands and possibly due to a change in oxidation state. The spectrum, however, returns to its original state after exposure to deuterated water thus showing reversible hydration-dehydration behavior for Mn(II) species in MnAPO-5.

The case of FeAPO-5 molecular sieve is more complex. As-synthesized as well as calcined, hydrated samples show a strong signal at $g = 4.25$ and a weak signal at $g = 1.99$ (Figure 2a). The ESR spectra of various iron-modified molecular sieves show three major signals at $g \approx 2.0$, $g \approx 2.2-2.3$, and $g \approx 4.3$. These various signals have been generally assigned to iron in ion-exchanged sites, iron in oxide or hydroxide phases, and iron in framework sites, respectively. The appearance of a signal at $g \approx 4.23$ has often been used as evidence for isomorphous framework substitution of iron. However, the validity of these assignments has been questioned as there are often inconsistencies with other characterization methods. In a recent study[30] of the local structure of Fe(III) in a series of ferrisilicate and ferrialuminosilicate zeolites, the assignments of the $g \approx 2.0$ and 4.3 signals were reversed. Fe−sodalite, Fe−L, Fe−faujasite, Fe−ZSM-5, and Fe−mazzite in which iron was incorporated during zeolite synthesis were studied by X-band (9 GHz) and Q-band (35 GHz) ESR and ESEM spectroscopies. A strong signal at $g \approx 2.0$ was observed in the ESR spectra of all Fe−zeolites, whereas a weak signal at $g \approx 4.3$ was observed only in Fe−faujasite, Fe−ZSM-5, and Fe−mazzite. Thus, the $g \approx 2.0$ signal is assigned to lattice-substituted, tetrahedral high-spin Fe(III) and the signal at $g \approx 4.3$ is interpreted as Fe(III) in a defect site where iron is coordinated to framework oxygens and to one or two terminal oxygens.[30] This interpretation was later supported in an ESR study of ferrisilicate and FeAPO-5 molecular sieves.[31] The $g \approx 4.3$ signal was assigned to Fe(III) in a distorted tetrahedral defect site and the $g \approx 2.0$ signal to tetrahedral Fe(III) in a framework site. This later assignment should be taken with caution since oxidic clusters of iron also exhibit a broad ESR signal near $g \approx 2.0$.

In the FeAPO-5 studied in this work, the intensity of the near $g \approx 4.3$ signal is significantly higher than that of the signal

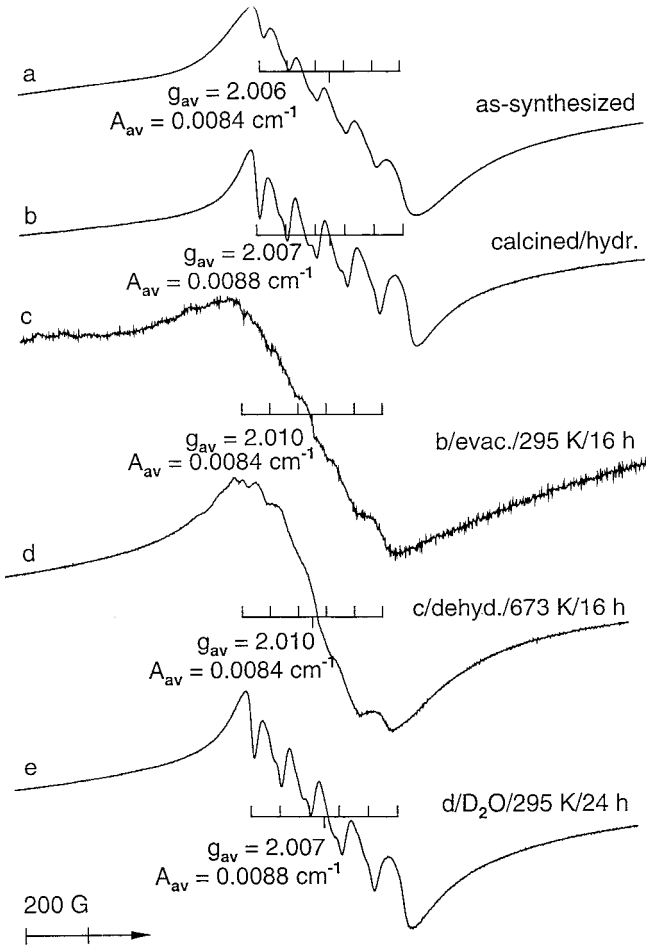

Figure 1. ESR spectra at 77 K of MnAPO-5 molecular sieve for (a) an as-synthesized sample, (b) a calcined, hydrated sample, (c) after evacuation of a calcined sample at 295 K for 16 h, (d) after dehydration of an evacuated sample at 673 K for 16 h, and (e) after adsorption of D_2O on a dehydrated sample at 295 K for 24 h.

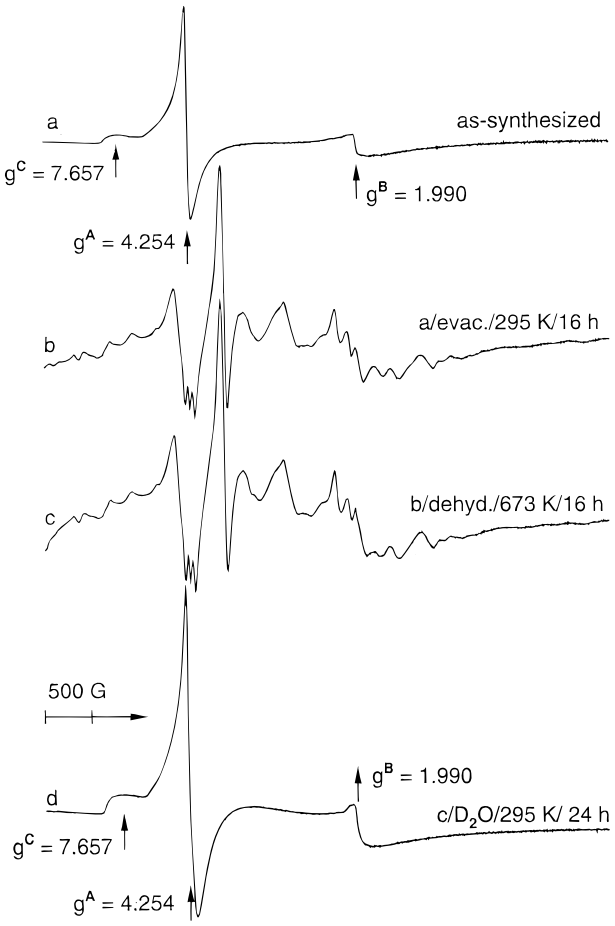

Figure 2. ESR spectra at 77 K of FeAPO-5 molecular sieve for (a) an as-synthesized sample, (b) after evacuation of a calcined sample at 295 K for 16 h, (c) after dehydration of an evacuated sample at 673 K for 16 h, and (d) after adsorption of D_2O on a dehydrated sample at 295 K for 24 h.

near $g \approx 2.0$. If these assignments are correct, the majority of iron incorporated into FeAPO-5 molecular sieve is in defect sites. A different ESR spectrum with multiple lines is observed upon evacuation of a calcined, hydrated sample (Figure 2b). The spectrum remains the same even after dehydration of the sample at 673 K for 16 h. The multiple lines may be a contribution from zero-field interaction.[32] Upon exposure of a dehydrated sample to deuterated water, the original spectrum of a calcined, hydrated sample is regained (Figure 2d). This shows that, as in MnAPO-5, the hydration−dehydration behavior in FeAPO-5 is reversible. Moreover, this is an indication that the location of Fe(III) in FAPO-5 is not changed during dehydration.

The as-synthesized, calcined, and dehydrated TAPO-5 and NiAPSO-5 materials do not show any ESR signal, suggesting that the metal ions are in nonparamagnetic Ti(IV) and Ni(II) oxidation states, respectively. After reduction of dehydrated samples with hydrogen (NiAPSO-5) or γ-rays (TAPO-5), the samples show characteristic ESR signals due to paramagnetic Ti(III) and Ni(I) ions. The ESR parameters of the various paramagnetic species in these materials that were investigated by ESEM are given in Table 2.

To simulate the ESEM spectra of the various MeAPO-5/MeAPSO-5 molecular sieves, it is necessary to analyze the first and second nearest neighbor distances of the framework elements in these materials. The AFI framework structure is given in Figure 3. The lattice parameters reported[32] for the AFI structure were taken as inputs to the program. Significant variations in interatomic distances and angles are reported for this structure. The P−O and Al−O interatomic distances vary over the ranges 1.45−1.52 Å and 1.68−1.73 Å, respectively. Similarly, the P−O−Al angle varies between 149° and 178°. So, average values of 3 Å and 150° were chosen as the mean T−T distance and T−O−T angle. A metal ion at a framework phosphorus site has four aluminum atoms as its nearest neighbor tetrahedral atoms. The next nearest neighbor tetrahedral sites are occupied by phosphorus atoms, which are distributed at various distances from 3.9 to 5.3 Å as shown in Figure 3. There is one phosphorus atom at 3.9 Å in the four-ring connecting the metal site. There are two phosphorus atoms at 4.8 Å in the six-ring connecting the metal site and lying in a plane perpendicular to the *c* axis. There are six phosphorus atoms at 5.1 Å in the planes above and below the plane containing the metal site. There are two phosphorus atoms at 5.3 Å in the 12-ring connecting the metal site for a total of 11 next nearest neighbor phosphorus atoms.

On the other hand, for a metal ion substituting for a framework aluminum site, there are four nearest neighbor phosphorus atoms at 3.0 Å. Figure 4 shows an experimental ^{31}P ESEM spectrum of dehydrated MnAPO-5 together with simulated curves for various sets of interacting phosphorus nuclei. The best-fit simulation curve (Figure 4b) is obtained for one phosphorus at 4.2 Å and two phosphorus at 5.8 Å. The best fit is determined by a computer program which systematically varies the parameters until the sum of the squared residuals between the simulated and experimental spectra is minimized. This curve is quite similar to the simulation curves for one phosphorus nucleus at 3.9 Å (Figure 4c) and for one phosphorus at 3.9 Å and two phosphorus at 4.8 Å (Figure 4d). This suggests that the major contribution to the echo modulation is from one phosphorus nucleus at ∼4 Å in the four-ring connecting the metal ion. If 10 phosphorus are added at an average second shell distance of 5.0 Å (Figure 4e) to complete the next nearest neighbor coordination sphere of 11 phosphorus nuclei, the overall modulation depth is significantly greater than in the experimental spectrum (Figure 4a). In fact, if 11 phosphorus nuclei are all positioned at average interaction distances from 5.0 to 5.3 Å (Figure 5) the overall modulation depth is greater than the experimental one. It appears that not all the next nearest neighbor phosphorus nuclei contribute to the modulation.

On the other hand, if one assumes that the metal ion substitutes for a framework aluminum site there are four nearest neighbor phosphorus at 3.0 Å. A simulation for these parameters is shown in Figure 4f and the calculated modulation curve is quite different from the experimental curve much more so than for metal ion substitution for a phosphorus site. Thus, the possibility of the metal ion substituting for a framework aluminum site seems highly unlikely.

The observations from the ^{31}P ESEM data that manganese ions are incorporated at framework phosphorus sites are further supported by ^{27}Al ESEM spectra recorded for MnAPO-5. Figure 6 shows the ^{27}Al ESEM spectrum measured for as-synthesized and dehydrated MnAPO-5 molecular sieves. The magnetic field was set at the same value as that used for ^{31}P modulation. The interpulse time was selected as 0.12 μs to minimize ^{31}P modulation. The strong aluminum modulation indicates the closer proximity of Mn(II) to aluminum than to phosphorus.

The incorporation of manganese into aluminophosphate MnAPO-20, which is structurally analogous to sodalite zeolite, has been investigated recently by electron nuclear double resonance (ENDOR) and electron spin−echo modulation spec-

TABLE 2: ESR Parameters of Various Paramagnetic Ions in MeAPO/MeAPSO-5 Molecular Sieve

sample	species	ESR parameters			reference
TAPO-5	Ti (III)	$g_1 = 1.965$	$g_2 = 1.920$	$g_3 = 1.879$	17
VAPO-5	V (IV)	$g_{\|\|} = 1.908$	$A_{\|\|} = 0.0189$ cm^{-1}		16
CrAPSO-5	Cr (V)	$g_{\|\|} = 1.890$	$g_\perp = 1.970$		18
MnAPO-5	Mn (II)	$g_{av} = 2.007$	$A_{av} = 0.0088$ cm^{-1}		this work
FeAPO-5	Fe (III)	$g^A = 4.254$	$g^B = 1.990$		this work
NiAPSO-5	Ni (I)	$g_{\|\|} = 2.519$	$g_\perp = 2.111$		10
CuAPO-5	Cu (II)	$g_{\|\|} = 2.612$	$g_\perp = 1.988$	$A_\perp = 0.0072$ cm^{-1}	27

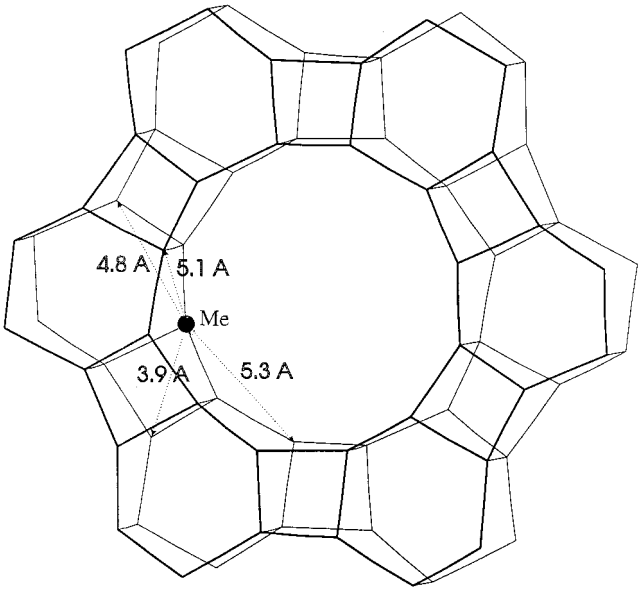

Figure 3. AFI structural model showing the variation in distance between a tetrahedral site Me and the second nearest neighbor tetrahedral sites to Me.

troscopies.[34] X-band ESEM measurements were performed on Mn(II) over a field range of 2220−3620 G to obtain information about the weak hyperfine interactions from surrounding nuclei. Modulations from framework ^{31}P and ^{27}Al nuclei as well as from extraframework nuclei ^{14}N and ^{1}H from a template molecule are variously observed in all spectra. Modulation from ^{31}P was dominant when the field was set between 2820 and 3020 G, while moderately strong ^{27}Al modulations are observed when the field was set at 2220−2820 G. The simulation of the time domain spectra was not given, so possible information about the number and interaction distances of ^{31}P from Mn(II) was not obtained by such a simulation procedure. However, evidence for incorporation of manganese at a framework aluminum site was suggested by the presence of a pulsed ENDOR doublet separated by about 8 MHz symmetrically flanking the Larmor frequency of ^{31}P at W-band at 34 kG, while no such doublet was observed in the region around the Larmor frequency of ^{27}Al. This doublet was assigned to an isotropic hyperfine interaction between Mn(II) and phosphorus. Since no such isotropic hyperfine was observed for Mn(II) with aluminum it was reasonably argued that Mn(II) is nearer to phosphorus than to aluminum. However, this conclusion is not consistent with our present ESEM results for MnAPO-5, where the ^{31}P and ^{27}Al ESEM data indicate that the manganese ion occupies a framework phosphorus site. Although AlPO-5 and AlPO-20 have different structures, it seems that consistent agreement about the Mn(II) site in AlPO materials is lacking.

The interpretation of the ^{31}P ESEM modulation of MnAPO-5 can be extended to the spectra observed for other MeAPO-5 and MeAPSO-5 molecular sieves. Figure 7 shows the observed and simulated ^{31}P ESEM spectra of various MeAPO-5/

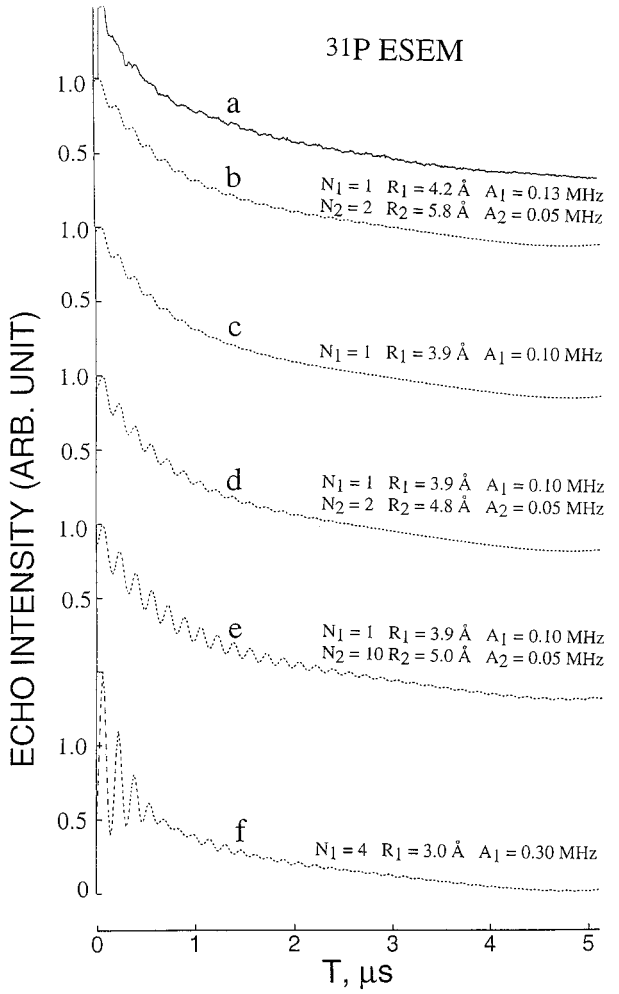

Figure 4. Experimental (—) three pulse ^{31}P ESEM spectrum of MnAPO-5 and simulations (· · ·) assuming various sets of interacting nuclei where N is the number of phosphorus nuclei interacting with Mn(II), R is the distance between Mn(II) and phosphorus with an estimated uncertainty of ±0.1 Å, and A is the isotopic hyperfine coupling constant with an estimated uncertainty of ±10%.

MeAPSO-5 samples. The observed ^{31}P ESEM spectra are generally weak. For FeAPO-5, no echo was observed when the field was set at $g = 4.25$ and very weak modulation was observed when the field was set at $g = 1.999$. This difference in echo modulation behavior suggests different origins for these two signals. The best-fit simulation parameters for the ^{31}P ESEM spectra given in various references are summarized in Table 3. It should be noted that two sets of parameters provide a simulation that accounts reasonably well for the experimental ^{31}P modulation. One set is one phosphorus near 4.0 Å and the other set is nine phosphorus near 5.1 Å. However, from Figure 3, one phosphorus near 4.0 Å seems most consistent with the AFI structure.

It should be mentioned that although there are variations in their decay behavior, the ^{31}P ESEM spectra for various MeAPO-

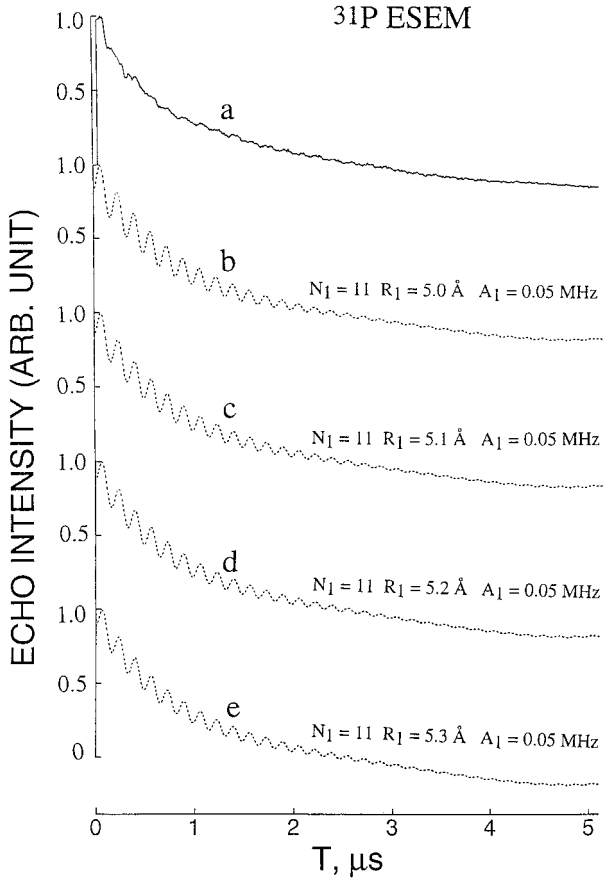

Figure 5. Experimental (—) three pulse ^{31}P ESEM spectrum of MnAPO-5 and simulations (· · ·) assuming 11 next nearest neighbor ^{31}P at distances from 5.0 to 5.3 Å.

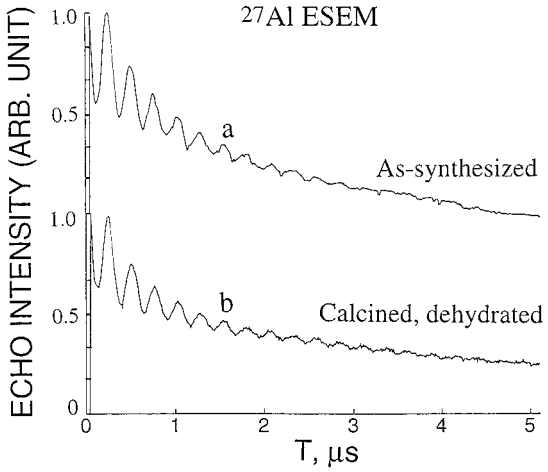

Figure 6. Experimental three pulse ^{27}Al ESEM spectrum of as-synthesized and calcined, dehydrated MnAPO-5.

5/MeAPSO-5 molecular sieves have essentially the same modulation depth. This suggests that the phosphorus environment around the metal ion in these materials is essentially the same irrespective of the particular metal ion. Otherwise, one would observe quite different ^{31}P ESEM spectra for a tetravalent metal such as Ti(IV) than from a divalent metal such as Mn(II). Chemical analysis supports that a tetravalent metal such as titanium substitutes for a framework phosphorus site and that a divalent metal such as manganese substitutes for an aluminum site.[9,35] Despite the fact that there are variations in the simulation parameters among individual metal ions, these parameters are most generally consistent for metal ion substitution at a framework phosphorus site. For a divalent metal ion such as Mn(II), this observation contrasts with earlier reports in which an aluminum site was suggested for its substitution.[9,34] The weak ^{31}P modulation and the uncertainty in reliably simulating such weak modulation indicate caution in definitive assignment to substitution at a phosphorus site.

From the ^{31}P ESEM studies of MeAPO/MeAPSO-5 molecular sieves, it can be concluded that these measurements are useful in obtaining information about metal ion incorporation into framework sites of MeAPO/MeAPSO molecular sieves, especially by comparison with materials where the metal ions are

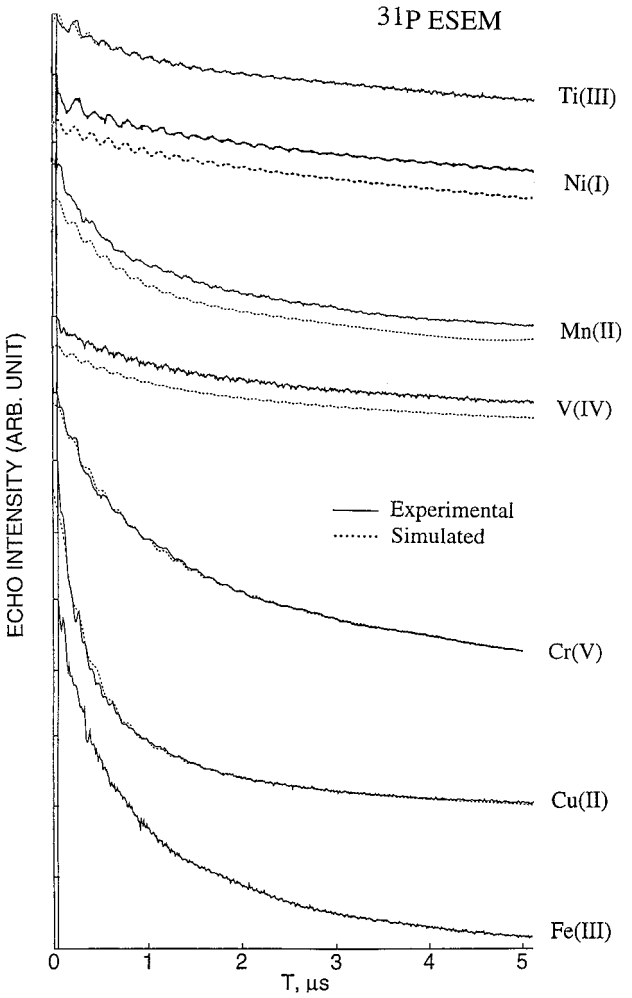

Figure 7. Experimental (—) and simulated (· · ·) three pulse ^{31}P ESEM spectra of (a) TAPO-5, (b) NiAPSO-5, (c) MnAPO-5, (d) VAPO-5, (e) CrAPSO-5, (f) CuAPO-5, and (g) experimental three pulse ^{31}P ESEM spectra of FeAPO-5 from top to bottom.

TABLE 3: Simulation Parameters of ^{31}P ESEM for Various Paramagnetic Ions in MeAPO/MeAPSO-5 Molecular Sieves

		ESEM simulation parameter			
sample	species	*N*	*R* (Å)	*A* (MHz)	reference
TAPO-5	T (III)	1	3.9	0.3	17
		2	4.8	0.1	
VAPO-5	V(IV)	1	4.4	0.3	16
CrAPSO-5	Cr(V)	9	5.2	0.1	18
MnAPO-5	Mn(II)	1	4.2	0.13	this work
		2	5.8	0.05	17
FeAPO-5	Fe(III)	no echo for signal at $g = 4.25$; very weak modulation for signal at $g = 1.999$			this work
NiAPSO-5	Ni(I)	8.8	5.1	0.1	10
CuAPO-5	Cu(II)	8.0	5	0.1	27

introduced into nonframework sites by ion-exchange or impregnation. It is interesting that the ESEM simulation parameters consistently indicate transition metal ion incorporation at phosphorus sites in MeAPO/MeAPSO materials.

Conclusions

Electron spin−echo modulation spectroscopy in combination with electron spin resonance spectroscopy were successfully employed to investigate the mode of incorporation of transition metal ions in various MeAPO-5 and MeAPSO-5 molecular sieves. Weak ^{31}P modulation is observed for transition metal ions Ti(III), V(IV), Cr(V), Mn(II), Fe(III), Ni(II), and Cu(II) in the corresponding molecular sieves TAPO-5, VAPO-5, CrAPSO-5, MnAPO-5, FeAPO-5, NiAPSO-5, and CuAPO-5. Simulations of these spectra suggest that irrespective of any particular metal ion, the ^{31}P ESEM spectra of MeAPO/MeAPSO molecular sieves can be interpreted best on the basis of metal ion incorporation at a framework phosphorus site. The strong ^{27}Al modulation observed for these materials supports that the metal ions are located nearer to aluminum than to phosphorus.

Acknowledgment. This research was supported by the National Science Foundation and the Robert A. Welch Foundation.

References and Notes

(1) Wilson, S. T.; Flanigen, E. M. U. S. Patent 4,567,029, 1986.
(2) Flanigen, E. M.; Lok, B. M.; Patton, R. L.; Wilson, S. T. *Pure Appl. Chem*. **1986**, *58*, 1351.
(3) Sheldon, R. A.; Dakka, J. *Catal. Today* **1994**, *19*, 215.
(4) Inui, T.; Phatanasri, S.; Matsuda, H. *J. Chem. Soc., Chem. Commun*. **1990**, 205.
(5) Wan, B.-Z.; Huang, K. *Appl. Catal*. **1991**, *73*, 113.
(6) Chen, J.; Thomas, J. M. *J. Chem. Soc., Chem. Commun.* **1994**, 603.
(7) Weckhuysen, B. M.; Rao, R. R.; Martens, J. A.; Schoonheydt, R. A. *Eur. J. Inorg. Chem.* **1999**, 565.
(8) Hartmann, M.; Kevan, L. *Chem. Rev*. **1999**, *99*, 635.
(9) Wilson, S. T.; Flanigen, E. M. In *Zeolite Synthesis*; Occelli, M. L., Robson, H. E., Eds.; ACS Symposium Series 398; American Chemical Society: Washington, DC, 1989; pp 329−345.
(10) Hartmann, M.; Azuma, N.; Kevan, L. *J. Phys. Chem*. **1995**, *99*, 10988.
(11) Prakash, A. M.; Harmann, M.; Kevan, L. *J. Chem. Soc., Faraday Trans.* **1997**, *93*, 1233.
(12) Djieugoue, M.-A.; Prakash, A. M.; Kevan, L. *J. Phys. Chem. B* **1999**, *103*, 804.
(13) Montes, C.; Davis, M. E.; Murray, B.; Narayana, M. *J. Phys. Chem.* **1990**, *94*, 6431.
(14) Jhung, S. H.; Uh, Y. S.; Chon, H. *Appl. Catal*. **1990**, *62*, 61.
(15) Rigutto, M. S.; van Bekkum, H. *J. Mol. Catal*. **1993**, *81*, 77.
(16) Prakash, A. M.; Kevan, L. *J. Phys. Chem. B* **1999**, *103*, 2214.
(17) Prakash, A. M.; Kurshev, V.; Kevan, L. *J. Phys. Chem. B* **1997**, *101*, 9794.
(18) Zhu, Z.; Kevan, L. *Phys. Chem. Chem. Phys*. **1999**, *1*, 199.
(19) Behrens, P.; Felsche, J.; Niemann, W. *Catal. Today* **1991**, *8*, 479.
(20) Xu, Y.; Couves, J. W.; Jones, R. H.; Catlow, C. R. A.; Greaves, G. N.; Chen, J.; Thomas, J. M. *J. Phys. Chem. Solids* **1991**, *52*, 1229.
(21) Tusar, N. N.; Tuel, A.; Arcon, I.; Kodre, A.; Kaucic, V. In *Progress in Zeolite and Microporous Materials*; Chon, H., Ihm, S.-K., Uh, Y. S., Eds.; Studies in Surface Science and Catalysis 105; Elsevier: Amsterdam, 1997; pp 501−508.
(22) Tuel, A.; Arcon, I.; Tusar, N. N.; Meden, A.; Kaucic, V. *Microporous Mater*. **1996**, *7*, 271.
(23) Zhang, G.; Harris, T. H. *Physica B* **1995**, *208/209*, 697.
(24) Radaev, S. F.; Joswig, W.; Baur, W. H. *J. Mater. Chem*. **1996**, *6*, 1413.
(25) Chao, K.-J.; Sheu, S.-P.; Sheu, H.-S. *J. Chem. Soc., Faraday Trans.* **1992**, *88*, 2949.
(26) Kevan, L. In *Modern Pulsed and Continuous-wave Electron Spin Resonance*; Kevan, L., Bowman, M. K., Eds.; Wiley: New York, 1990; pp 231−266.
(27) Munoz, T.; Prakash, A. M.; Kevan, L.; Balkus, K. J., Jr. *J. Phys. Chem. B* **1998**, *102*, 1379.
(28) Goldfarb, D. *Zeolites* **1989**, *9*, 509.
(29) Rubio, J. O.; Munoz, E. P.; Boldu, J. O.; Chen, Y.; Abraham, M. M. *J. Phys. Chem.* **1979**, *70*, 633.
(30) Goldfarb, D.; Bernardo, M.; Strohmaier, K. G.; Vaughan, D. E. W.; Thomann, H. *J. Am. Chem. Soc*. **1994**, *116*, 6344.
(31) Catana, G.; Pelgrims, J.; Schoonheydt, R. A. *Zeolites* **1995**, *15*, 475.
(32) Castner, T.; Newal, G. S.; Holton, W. C.; Slichter, C. P. *J. Chem. Phys.* **1960**, *32*, 668.
(33) Bennett, J. M.; Cohen, J. P.; Flanigen, E. M.; Pluth, J. J.; Smith, J. V. In *Intrazeolite Chemistry*; Stucky, G. D., Dwyer, F. G., Eds.; ACS Symposium Series 218; American Chemical Society: Washington, DC, 1983; pp 109−118.
(34) Ariell, D.; Vaughan, D. E. W.; Strohmaier, K. G.; Goldfarb, D. *J. Am. Chem. Soc.* **1999**, *121*, 6028.
(35) Marchese, L.; Prache, A.; Coluccia, S.; Thomas, J. M. In *Proceedings of the 12th International Zeolite Conference*; Treacy, M. M. J., Marcus, B. J., Bisher, M. E., Higgins, J. B., Eds.; Materials Research Society: Warrendale, PA, 1999; pp 1569−1576.